Running head: Face-centered representations

IN PRESS: CURRENT BIOLOGY

Face-specific perceptual distortions reveal a view- and orientation-independent face template

Jorge Almeida[1,2,*], Andreia Freixo[1,2,¥], Miguel Tábuas-Pereira[3,4,¥], Sarah B. Herald[5], Daniela Valério[1,2], Guilherme Schu[1,2], Diana Duro[3,4,6], Gil Cunha[3,4,6], Qasim Bukhari[1,2,7], Brad Duchaine[5*] & Isabel Santana[3,4,6]

1. Proaction Laboratory, Faculty of Psychology and Educational Sciences, University of Coimbra. Coimbra 3000-115, Portugal
2. CINEICC, Faculty of Psychology and Educational Sciences, University of Coimbra. Coimbra 3000-115, Portugal
3. Neurology Department and Dementia Clinic, Centro Hospitalar e Universitário de Coimbra. Coimbra 3000-075, Portugal.
4. Centre for Neuroscience and Cell Biology (CNC), University of Coimbra. Coimbra 3004-504, Portugal.
5. Psychological and Brain Sciences, Dartmouth College. Hanover, NH 03755, USA
6. Faculty of Medicine, University of Coimbra. Coimbra 3004-504, Portugal.
7. McGovern Institute for Brain Research, Massachusetts Institute of Technology. MA 02139, USA.

*Correspondence should be sent to:
Jorge Almeida, Proaction Laboratory, Faculty of Psychology and Educational Sciences, University of Coimbra. Coimbra 3000-115, Portugal. jorgecbalmeida@gmail.com
Brad Duchaine, Psychological and Brain Sciences, Dartmouth College, Hanover, NH 03755, USA. bradley.c.duchaine@dartmouth.edu
¥ These authors contributed equally to this paper.

Lead Contact:
Jorge Almeida, Proaction Laboratory, Faculty of Psychology and Educational Sciences, University of Coimbra. Coimbra 3000-115, Portugal. jorgecbalmeida@gmail.com

Summary
The spatial coordinate system in which a stimulus representation is embedded is known as its reference frame. Every visual representation has a reference frame [1], and the visual system uses a variety of reference frames to efficiently code visual information [e.g., 1, 2, 3-5]. The representation of faces in early stages of visual processing depends on retino-centered reference frames, but little is known about the reference frames that code the high-level representations used to make judgements about faces. Here we focus on a rare and striking disorder of face perception – hemi-prosopometamorphopsia (hemi-PMO) – to investigate these reference frames. Following a left splenium lesion, Patient A.D. perceives features on the right side of faces as if they had melted. The same features were distorted when faces were presented in either visual field, at different in-depth rotations, and at different picture-plane orientations including upside-down. A.D.'s results indicate faces are aligned to a view- and orientation-independent face template encoded in a face-centered reference frame, that these face-centered representations are present in both the left and right hemisphere, and that the representations of the left and right halves of a face are dissociable.

Keywords
Face processing; Hemi-Prosopometamorphopsia; View-independent face representation; Splenium;

Face-centered representations

Highlights

- After a left splenium lesion, A.D. sees features in right face halves as distorted
- A.D.'s distortions affect the same features under all stimulus manipulations tested
- Face processing involves a view- and orientation-independent face template
- The face vertical midline is an important representational divide in face processing

In Brief

After a left splenium lesion, patient A.D. sees the right halves of faces as melting. Almeida et al. show that the distortion affects the same features regardless of position, rotation in-depth, or in-plane inversion, indicating that faces are encoded in a view- and orientation independent manner.

Results

Studies of word neglect and object neglect have demonstrated the existence of three types of reference frames in high-level visual processing: 1) retino-centered reference frames that are centered on the visual field (e.g. Figure 1A), 2) stimulus-centered reference frames that are centered on the object or word being represented (e.g. Figure 1B), and 3) object-centered (or word-centered) reference frames that are also centered on the object or word being represented but the stimulus representation is rotated and scaled to match a standard template (e.g. Figure 1C) [2-5]. Face-centered reference frames, a face-specific version of object-centered reference frames, have been proposed in many models of human face processing [6, 7] and are used in machine face recognition systems [8, 9]. In these models, faces seen at different viewpoints, sizes, and positions in the visual field are aligned to a single template. The face-centered representations generated by such a template can then be compared to stored face-centered representations to determine identity, expression, and other characteristics. However, evidence for such face-centered representations in the human visual system is minimal [7].

Hemi-prosopometamorphopsia (hemi-PMO) is an extraordinary condition in which brain-damaged patients perceive one side of the face as distorted, with features that appear out of proportion, drooping, or swollen [10, 11]. Hemi-PMO results from disruptions to representations coded within a particular reference frame (e.g., retino-, stimulus-, face-centered), and the reference frame involved can be identified by examining how the distortion manifests when faces are presented in particular ways. Specifically, if hemi-PMO is caused by a disruption to one side of a retino-centered reference frame, then distortions would be expected to affect any portion of a face that is in the disrupted region of the visual field (Figure 1A). In contrast, stimulus-centered and face-centered frames, if they exist, are allocentric and thus not influenced by the position of the stimulus in the visual field. Hemi-PMO resulting from disruption to stimulus-centered representations would be expected to affect the same side of the face stimulus regardless of the orientation of the face (Figure 1B). Finally, if hemi-PMO is caused by problems with face-centered representations, distortions would affect the same facial features regardless of how the face was presented (Figure 1C). These different predicted patterns of distortions provide an opportunity to identify reference frames used in face perception, but none of the approximately 25 hemi-PMO case reports have investigated these predictions.

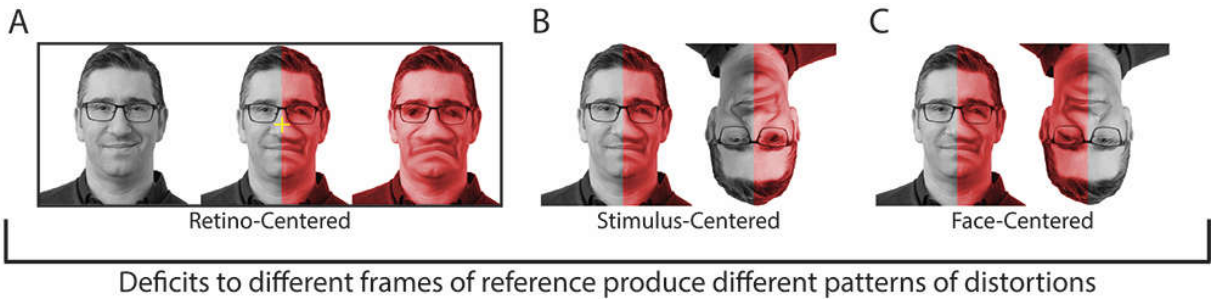

Figure 1. Hemi-PMO distortions and face-related reference frames. Predicted location of distortion (red) for different representational accounts. These examples show the distortion on the right in the upright face at fixation (consistent with A.D.'s distortions), but distortions in

hemi-PMO also occur on the left. **A**) In the retino-centered account, distortions are fixation-dependent and always right of fixation (yellow cross). For the two higher-level accounts, visual field position is irrelevant. **B**) The stimulus-centered account predicts distortions to the right side of the face stimulus. **C**) The face-centered account predicts distortions will affect the same facial features regardless of face orientation.

A.D.'s Case Description

A.D. is a right-handed man who was 59-years-old when he suddenly noticed one side of all the faces on his television were distorted. A.D. then looked in a mirror, and his own face showed the same distortion. The eye, nose, and corner of the mouth on the right side of the face from A.D.'s perspective (i.e., left side of the face being viewed) appeared as if they were melting. Throughout the paper, we will use A.D.'s perspective when referring to the side of a face. Hemi-PMO is a difficult condition to study because in most cases it does not persist [10, 11], but A.D.'s face distortions have persisted for more than six years. Not surprisingly, he finds it unpleasant to look at faces. A.D. has not noticed distortions in objects or other body parts. A neuropsychological exam showed no general cognitive impairments, normal visual acuity, and normal scores on a test of facial identity and facial expression discrimination (STAR Methods).

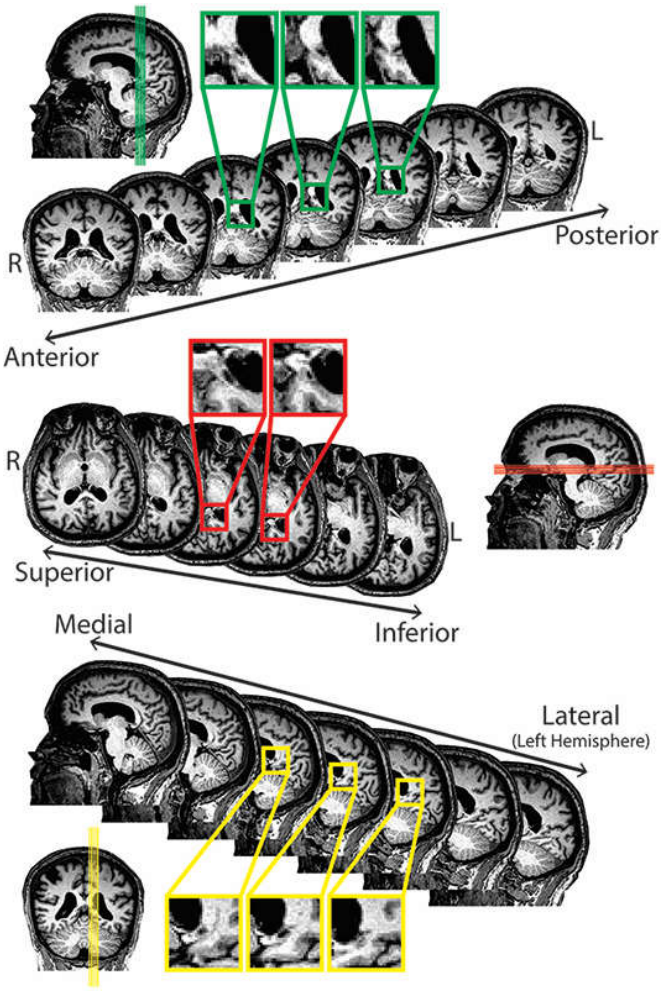

Figure 2. A.D.'s lesion. MRI structural scans in native space. Insets show detailed images of the lesion. The lesion is located in the left hemisphere splenium.

Like the majority of published hemi-PMO cases [11], A.D. has a lesion in the splenium (the posterior portion of the corpus callosum). His lesion affected the left side of the splenium (Figure 2), and its specificity was confirmed with DTI showing decrements in diffusion in the forceps major fiber bundle but not in other major fiber bundles (Figure S2).

Distortions occur across viewpoints and are specific to faces

In Experiment 1, we assessed which stimuli produce perceptual distortions in A.D. by presenting him with 20 images of human faces and 20 non-face images comprising objects, houses, cars, and geometrical shapes (Figure 3A). Face viewpoints ranged from full left profile (i.e. entire right side of face visible) to full right profile. A.D. reported distortions in 17 of the 20 faces (always on the right side) but none of the non-faces (Figure 3B; Figures S1 displays all images along with A.D.'s reports for each image).

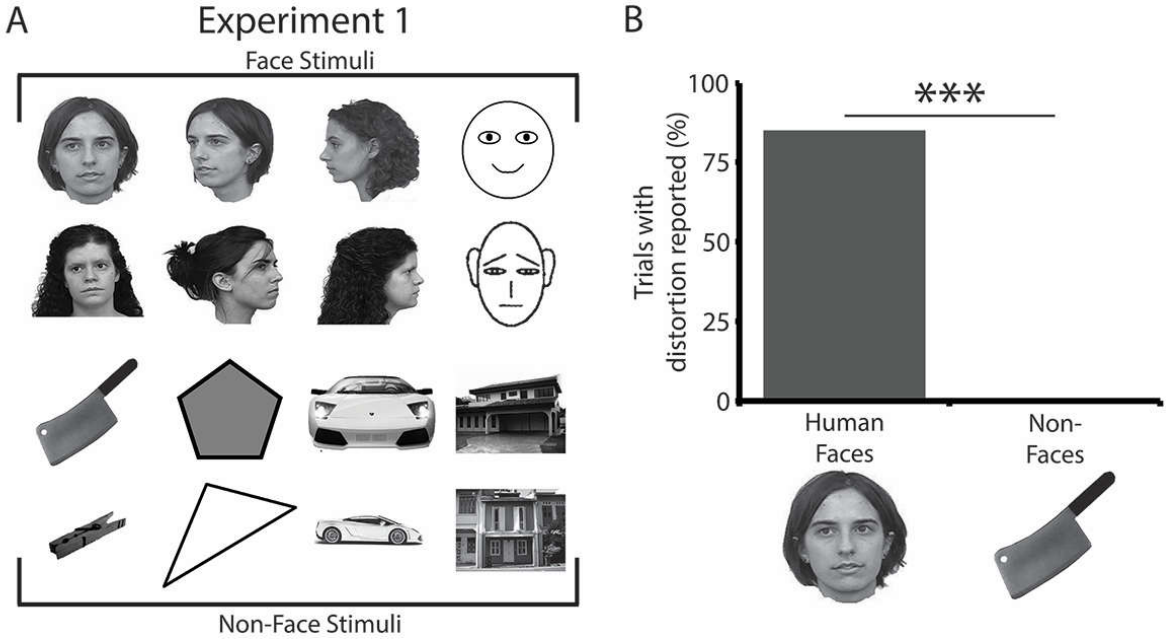

Figure 3. Stimulus examples and results of Experiment 1. A) Example stimuli. **B)** Percentage of trials in which A.D. reported a distortion. ***$p < 0.001$, Bonferroni corrected. See Table S1 for data and statistics. See Figure S1 for the stimuli and descriptions of the distortions reported by A.D..

For example, when presented with the face in the top left corner of Figure 3A, A.D. reported that the face parts on the right side of the face were longer, tighter, and fallen. The distortions were present in all but one of the views in which the right side of the face was easily visible (see Table S1 for statistics). These findings demonstrate that A.D. perceives distortions across the full range of in-depth rotations for which the right side of the face is visible and that A.D.'s distortions are face-specific.

A.D.'s distortions are caused by a disruption to a face-centered reference frame

If A.D.'s distortions reflect disruptions to the right side of a retino-centered representation (Figure 1A), they would cause distortions to faces presented in the right but not the left visual field. Alternatively, if the distortions are tied to the right side of the face stimulus (stimulus-centered account, Figure 1B) or to specific features that correspond to the right side of an upright face (face-centered account, Figure 1C), A.D. would perceive distortions in both visual fields. To test these predictions, A.D. was shown faces in both visual fields (Figure 4A). Consistent with the stimulus-centered and the face-centered accounts, A.D. showed no difference between visual fields (Figure 4B). He perceived distortions on the right side of the face in all nine faces presented in the left visual field and six of seven presented in the right visual field.

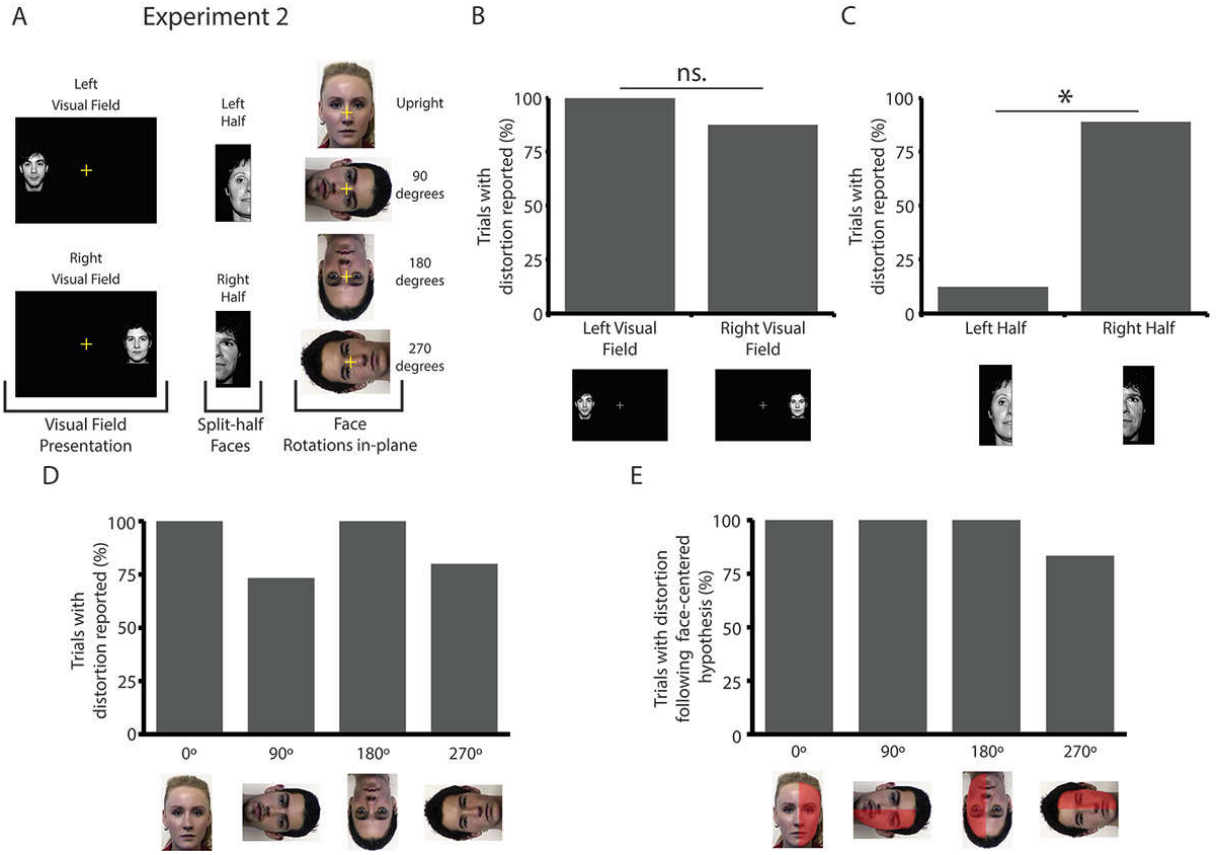

Figure 4. Stimulus examples and results of Experiment 2. A) Example stimuli. **B-D)** Percentage of trials in which A.D. reported a distortion for **B)** faces in left versus right visual field, **C)** left versus right face halves, and **D)** faces rotated in-plane. **E)** Of the trials for which A.D. saw a distortion in (D), all but two distortions were to features corresponding to the right side of the upright face. *$p < 0.05$, Bonferroni corrected. See Table S1 for data and statistics.

To distinguish between the face-centered and the stimulus-centered accounts, A.D. was presented with left-half and right-half faces at different locations in the visual field (Figure 4A).

Face-centered representations

The stimulus-centered account predicts distortions will be present on the right-hand side of both left halves and right halves, whereas if his distortions result from impairments to face-centered representations, he will perceive distortions to right halves but not the left halves. A.D. saw the distortions in all but one of the right halves and in only one of the left halves (Figure 4C), consistent with the face-centered account. The only distortion reported for a left-half face was perceived in the tip of the nose, perhaps because A.D. represented the tip as being part of the right side of the face.

To further test the predictions of these two accounts, A.D. was shown 15 frontal views of faces at each of four picture-plane orientations: 0° (upright), 90°, 180°, and 270° (Figure 4A). With these rotations, the same facial features (e.g., right eye) would be presented in different positions. For example, at 0° the right eye would be in the right visual field and on the right side of the stimulus whereas at 180° it would be in the left visual field and on the left side of the stimulus. A.D. perceived distortions in the majority of the faces at each orientation (Figure 4D), and, consistent with the face-centered account, he saw distortions in the same set of facial features (e.g., the right eye irrespective of rotation; Figure 4E) in all but two trials (270° condition).

To better understand A.D.'s distortions, we counted how often he reported distortions for a particular feature across all trials. He saw distortions in 96 faces (94 human faces + 2 animal faces). He reported a total of 210 distorted features in those faces because multiple features were distorted in the majority of the faces. The right eye was the feature A.D. saw distortions in most often (39% of the 94 images). The distortions affected the right side of the lip in 31% of the distorted faces and the right side of the nose in 29%. A.D. saw distortions affecting the left eye in one trial (a 270° rotated face; 0.5%), the left side of the nose in another trial (a left-half face; 0.5%), and the left side of the lip in a third trial (a 270° rotated face; 0.5%). When A.D. reported how a feature was distorted, it was almost always seen as melting down, but A.D. saw one nose as pulled up and the lip were pulled up in another face. In some eye distortions, A.D. reported the sclera was larger or whiter than normal, and in one upright face, the right eyebrow appeared to cover the right eye. Finally, in the non-upright presentations, A.D. reported that the distortions were weaker than in the upright presentations. In the 90° and 270° conditions, about half were weaker, and in the 180° condition, two out of 15 were weaker.

Discussion

The results from A.D. indicate that the human visual system contains procedures that encode faces in a face-centered frame of reference. A.D. did not see distortions in any non-face stimuli, so these processes are engaged only by faces. The persistence of A.D.'s distortions across viewpoints, so long as the right side of the face was visible, demonstrates that representations of different in-depth rotations are aligned to a common template. Interestingly, the same facial features were distorted in faces at different orientations including upside-down. This consistency suggests that although psychophysical [12] and neuropsychological evidence [13] indicate upright and upside-down face processing depend on qualitatively different procedures, both orientations are represented by the same face-centered reference frame at some point in the face system as a few neuropsychological results have implied [13, 14]. It is worth noting

that because the face system likely utilizes multiple reference frames [15], we expect hemi-PMO cases with different distortion profiles occur. Indeed, two hemi-PMO cases may have resulted from impairment to representations in a stimulus-centered reference frame rather than a face-centered frame. When shown a face rotated in the picture-plane, the patients' distortions continued to affect the same side of the stimulus and hence no longer affected the features distorted in upright faces [similar to Figure 1B; 16, 17].

Like many cases of hemi-PMO, A.D.'s distortions were caused by a lesion to the splenium. This lesion led to severe and specific diffusion deficits to the fibers that traverse the splenium and allow for the interhemispheric transmission of information between posterior temporal and occipital regions (the forceps major fiber bundle, see Figure S2). Because A.D.'s distortions reflect a disruption to information transmission from one hemisphere to the other, his case shows that both the left and the right hemisphere contain face-centered representations of the right side of the face. We suspect A.D.'s lesion interrupted transmission of face information from the left to the right hemisphere rather than vice versa because microstimulation to face areas in the right hemisphere produces conscious visual distortions more often than comparable left hemisphere stimulation [18] and MEG findings indicate face information from the left and right hemisphere converge in right fusiform gyrus [19]. It is also worth noting that the boundary between distorted and undistorted regions of the face in hemi-PMO is consistently seen along the vertical midline of the face (i.e., the line that runs between the eyes and splits the nose and mouth) and not the horizontal midline [11]. This asymmetry suggests that the vertical midline may be a critical division in face representation.

A.D.'s results also provide insight into the influence of face-centered representations on conscious perception. When we view faces, we are consciously aware of view-specific representations (e.g., frontal, left profile, etc.), and we do not have direct access to face-centered representations. Nevertheless, A.D. perceives the features in the view-specific representations that he is aware of as distorted. Because those distortions are generated by a face-centered representation, A.D.'s case indicates that output from the view-independent template can influence conscious percepts of faces, possibly through the substantial recurrent processing that occurs in the face network [20].

Interestingly, A.D. reported fewer distortions overall for the 90° and 270° rotation conditions in Experiment 2. Moreover, for half of the trials in which he reported the presence of the distortion in these conditions, he also reported that the distortions were weaker than usual. Inspection of A.D.'s verbal descriptions of the distortions also show that the 180° elicited weaker distortions than those he typically experiences for upright faces. In addition, counts of the number of times eyes, nose, or mouth were distorted in each condition (15 trials x 3 features = 45 maximum features to report) revealed fewer features were distorted in the inverted faces (N= 34) than in the upright faces (N= 42). Finally, on two trials in 270° condition, A.D. reported distortions on the left side of the face (left lip once, left eye in the other). These results suggest faces rotated away from upright are more difficult for the face system to align to the face-centered template, possibly because earlier levels of face representation are tuned to upright faces [12, 21].

Face-centered representations

More broadly, our study suggests commonalities in the processing of different visual categories. In the case of faces, A.D.'s results demonstrate the existence of face-centered reference frames, whereas the two hemi-PMO cases mentioned above who had distortions that affected a particular side of the face rather than particular features tentatively suggest face processing also involves stimulus-centered reference frames [16, 17]. Additional evidence for stimulus-centered face encoding is provided by a thoroughly tested patient with facial neglect whose recognition deficits were restricted to the right-hand side of the face stimulus regardless of orientation [15]. Similarly, studies of patients with neglect dyslexia have demonstrated that word-centered and stimulus-centered reference frames contribute to word processing. The operation of word-centered frames is revealed by cases of neglect dyslexia in which the same part of the word (i.e. first or second half) is neglected irrespective of whether the word is presented horizontally, backwards, or vertically [2-4], similar to A.D.'s face-centered deficit. Stimulus-centered coordinate frames are implicated by cases of neglect dyslexia in which the word half that is neglected depends on where it is located in the stimulus [e.g., for the word *deaf*, it might be read as *deal*, but if presented mirror-reversed it might be read as *leaf*; 4]. Thus, even though the category-specificity of hemi-PMO and neglect dyslexia demonstrates that face and word processing rely on different mechanisms, both processes appear to involve the same types of reference frames.

Acknowledgements
This work was supported by a Foundation for Science and Technology of Portugal and Programa COMPETE grant (PTDC/MHC-PCN/0522/2014) and a European Research Council (ERC) – under the European Union's Horizon 2020 Research and Innovation Programme – Starting Grant "ContentMAP" 802553 to JA. QB is supported by a Foundation for Science and Technology of Portugal and Programa COMPETE grant (PTDC/MHC-PCN/6805/2014). SH is supported by a National Science Foundation Graduate Research Fellowship. We thank Joana Nogueira and Stephanie Kristensen for their help in data collection.

Author contributions
J.A. conceived and designed the study. I.S., M.T.P. G.C. and A.F. tested the patient and collected the data. A.F., Q.B., G.G., D.V., S.H., and J.A. analyzed the data. J.A., B.D., and S.H. wrote the manuscript. All authors approved the final version of the manuscript.

Declaration of interests
The authors declare no competing interests.

Face-centered representations

Figure Legends

Figure 1. Hemi-PMO distortions and face-related reference frames. Predicted location of distortion (red) for different representational accounts. These examples show the distortion on the right in the upright face at fixation (consistent with A.D.'s distortions), but distortions in hemi-PMO also occur on the left. **A**) In the retino-centered account, distortions are fixation-dependent and always right of fixation (yellow cross). For the two higher-level accounts, visual field position is irrelevant. **B**) The stimulus-centered account predicts distortions to the right side of the face stimulus. **C**) The face-centered account predicts distortions will affect the same facial features regardless of face orientation.

Figure 2. A.D.'s lesion. MRI structural scans in native space. Insets show detailed images of the lesion. The lesion is located in the left hemisphere splenium.

Figure 3. Stimulus examples and results of Experiment 1. A) Example stimuli. **B)** Percentage of trials in which A.D. reported a distortion. ***$p < 0.001$, Bonferroni corrected. See Table S1 for data and statistics. See Figure S1 for the stimuli and descriptions of the distortions reported by A.D..

Figure 4. Stimulus examples and results of Experiment 2. A) Example stimuli. **B-D)** Percentage of trials in which A.D. reported a distortion for **B)** faces in left versus right visual field, **C)** left versus right face halves, and **D)** faces rotated in-plane. **E)** Of the trials for which A.D. saw a distortion in (D), all but two distortions were to features corresponding to the right side of the upright face. *$p < 0.05$, Bonferroni corrected. See Table S1 for data and statistics.

STAR METHODS

RESOURCE AVAILABILITY

LEAD CONTACT

Further information and requests for resources should be directed to and will be fulfilled by the Lead Contact, Jorge Almeida (jorgealmeida@fpce.uc.pt).

MATERIALS AVAILABILITY

This study did not generate new unique reagents.

DATA AND CODE AVAILABILITY

The datasets supporting the current study have deposited in a public repository. You can find it here: 10.6084/m9.figshare.12514673.

EXPERIMENTAL MODEL AND SUBJECT DETAILS

Participants.

Patient with hemi-PMO

At age 59, A.D. came to the Neurology Department of the *Centro Hospitalar e Universitário de Coimbra* complaining of suddenly seeing distortions in the right halves of people's faces, including his own face reflected in the mirror (right side from the perspective of the patient). He reported that the right eye, right side of the nose, and the right corner of the mouth look like they were "melted down" and that the two halves of the face did not fit together. No distortions in other parts of the body or in other objects were reported. There is no record of relevant medical history or medication prior to his visit. A CT-scan showed a hypointense lesion in the left splenium of the corpus callosum. MRI showed a T1 hypointense left splenium lesion, which was hyperintense in DP/T2 and FLAIR. Five months later, another MRI scan showed central necrosis of the lesion but no increase in size. A DTI scan carried out then indicated a reduction in the fractional anisotropy on the left side of the splenium. A.D. was suspected to have Marchiafava-Bignami disease resulting from vitamin deficiencies.

At the time of the current study when A.D. was 62, MRI and DTI scans were carried out (Figure 1, S2). A.D. also underwent a thorough neuropsychological exam that revealed no general impairments. In the Mini-Mental State Examination [MMSE; 22, Portuguese version: 23], A.D. scored 28 points which is normal for his age and education [Normative data for Portuguese population: 24]. He also showed no alexia/dyslexia, color anomia or changes in color perception (Ishihara 16/16), optic aphasia, agraphia, or other cognitive deficits. His visual acuity was normal (10/10 right eye; 9/10 left eye). A.D.'s face processing abilities were assessed with the Benton Facial Recognition Task [25] and the Comprehensive Affect Testing System [CATS; 26]. A.D. achieved a normal score on the Benton Facial Recognition Test (46/54; normal range between 41 and 54). On the CATS he showed no evidence of face discrimination deficits (emotion and identity) but revealed slight difficulty in the discrimination of vocal emotional prosody. It is worth noting that patients with hemi-PMO usually have no deficits with face recognition, possibly

because the undistorted face halves are sufficient for identity recognition. Finally, A.D. underwent a typical face localizer fMRI scan and showed face selectivity in posterior occipitotemporal regions (see Figure S3).

Controls

To assess A.D.'s deficit in white matter within the splenium, we recruited 50 controls to participate in a DTI experiment. Their age ranged between 61 and 79 years (average age: 69 years; SD = 5 years). All were native Portuguese speakers and had no history of neurological or psychiatric disorders.

The study adhered to the Declaration of Helsinki and was approved by the Ethics Committee of the Faculty of Psychology and Educational Sciences of the University of Coimbra. All participants (A.D. and controls) gave written informed consent after a detailed description of the complete study.

METHOD DETAILS

Behavioral Experiments: Stimuli and Procedure.

In Experiment 1, still images were used to assess whether A.D.'s distortions were restricted to faces or also affected other categories (Figure S1 displays each stimulus). These images included 20 human face stimuli which consisted of 15 unique photographs obtained from the Tarrlab at Carnegie Mellon University [27] (one face photograph was inadvertently presented twice, and thus the total number of faces was 16), and four schematic human faces. The image set also contained 20 non-face items obtained from the Internet such as cars (frontal and side views), tools, houses, and geometric shapes. A.D. was also shown eight photographs of animals, six of which included the animal's faces. Because it is uncertain whether animal faces engage the mechanisms that normally process human faces, we did not combine the human face and animal face results. For Experiment 2, we used a set of human faces from the Stirling face database (pics.stir.ac.uk) that were rotated in plane or split in half (as shown in Figure 2A).

In Experiment 1, the human faces, non-face items, and animals were interleaved with each other. The 48 images were presented until A.D. reported the presence or absence of a distortion and where on the image it occurred. Experiment 2 consisted of 93 trials, with the trials for the three different manipulations interleaved. As in Experiment 1, A.D. reported the presence or absence of a distortion and where it occurred. To examine the effect of face orientation, 60 trials consisting of 15 faces presented at four in-plane rotations (0, 90, 180, 270 degrees) were displayed centrally. On 16 trials, a full frontal upright face was presented in either the left or right visual field in three different locations in each field – up, center, and down – while A.D. fixated centrally. Left or right half faces were presented in another 17 trials along the azimuth, either centrally or in the left or right visual field. A.D. responded shortly after each image was presented in both experiments. A.D. finds looking at faces unpleasant; thus, the experiments were kept short.

QUANTIFICATION AND STATISTICAL ANALYSIS

Behavioral Experiments

Because the schematic faces are representations of human faces, we grouped them together with the human faces for the analysis and in Figure 2. Animals were kept as a separate category for the analysis because they are not human faces. They were excluded from Figure 2 due to the heterogeneity of the set (e.g., some are cropped images of faces, some of faces and bodies, and one is a butterfly with no discernible face), which makes the aggregate result for the group difficult to interpret. Tools, cars, geometric shapes, and houses were all grouped together as non-face stimuli.

A two-sided Fisher's exact test was used for all statistical comparisons. For each comparison, we created a 2x2 contingency table consisting of the number of times a distortion was reported or was not reported for the two conditions. The data for these tests along with the calculated *p*-values can be found in Supplemental Table 1. All tests were run in R [R Core 28] version 3.6.1 using the function stats::fisher.test() with all of the default arguments. Fisher's exact test was used instead of the Chi-squared test because some of the cells in our 2x2 contingency tables had few or no observations [29]. Fisher's exact test assumes fixed marginals, an assumption that was violated because we did not tell A.D. how many distortions to report. The importance of this assumption, however, has been strongly contested, and several statisticians, including Fisher himself, have argued that Fisher's exact test is appropriate even if only one margin is fixed [30]. Thus, we believe that Fisher's exact test is valid for our data, that it is a more appropriate statistical test than the Chi-squared test, and that its simplicity makes it a better choice than more exotic alternatives.

MRI Data

MRI data were acquired on a 3T MAGNETOM Trio whole-body MR scanner using a standard 12-channel head coil. Structural MRI data were acquired using a T1-weighted magnetization prepared rapid gradient echo sequence (repetition time (TR) = 2530 ms, echo time (TE) = 3.29 ms, flip angle (α) = 7°, field of view (FoV) = 256 × 256, matrix size = 256 × 256, bandwidth (BW) = 200 Hz/px, parallel acquisition technique GRAPPA acceleration factor 2).

DTI Data and processing

DTI data were acquired on the same 3T MAGNETOM Trio whole body MR scanner using a single shot echo-planar sequence (60 diffusion directions, TR/TE=8900/86 ms, b = 1000 s/mm2, 70 slices with resolution of 2×2×2 mm, 10 non-diffusion weighted volumes).

We followed the diffusion preprocessing pipeline available in the MRDIFFUSION module of the Vistasoft package, developed in the VISTA lab at Stanford University (https://github.com/vistalab/vistasoft). First, the acquired diffusion weighted images were converted from DICOM to NIFTI. Next, patient motion and eddy current distortions were corrected via non-linear co-registration, combining a rigid body transformation (with 6 parameters) with a constrained non-linear warping (with 8 parameters), estimated from an eddy-current distortion model [31]. This procedure uses SPM5 [32] optimization routines to estimate the parameters of the model, maximizing the normalized mutual information between each

diffusion image and the mean of the 10 non-diffusion weighted images. Diffusion tensor fitting was then estimated using a least-square optimization approach, which allowed us to compute eigenvalue-based measures, and specifically fractional anisotropy (FA) and radial diffusivity (RD). Both these measures can be computed by diagonalizing the diffusion tensor of each voxel in the image volume and have been widely used to characterize the diffusion displacement in the microstructure of white matter [33]. The FA measure is equal to the normalized standard deviation of the eigenvalues of the fitted tensor and, in non-crossing fibers regions, can be interpreted to reflect how eccentric the shape of the covariance of the diffusion propagation function is in a given voxel. The higher (closer to 1) the FA value, the higher is the association of that voxel with anisotropic diffusion displacement (e.g., diffusion displacement is constrained by fiber bundles). The RD measure is the mean of the second and third largest eigenvalues (i.e. these eigenvalues are associated with the basis vectors perpendicular to the major principal direction of diffusion) and studies have suggested that an increase in RD is associated with axon demyelination [34].

Tractography was then carried out using the automatic fiber quantification (AFQ) method [35; package available at https://github.com/yeatmanlab/AFQ]. First, whole brain tractography was carried out using the STT deterministic streamlines tracking algorithm [36], with an FA threshold value of 0.2 and angle threshold equal to 30°. Afterwards, four subgroups of tracts were segmented using an automated version of the methodology [37], namely: the forceps major, the forceps minor, the left and right inferior fronto-occipital fasciculi and the left and right inferior longitudinal fasciculi (see Figure S2 for the FA and RD results). The segmented fasciculi were then refined by comparing the obtained fasciculi with a probabilistic white matter atlas and cleaned by removing fibers that deviated greatly (in terms of the Mahalanobis distance) from the mean core tract. With the AFQ approach, a fiber bundle is resampled in 100 equidistant nodes and the mean core tract can be computed by averaging each fiber's x, y, and z coordinates at each node. Finally, using the AFQ method, we computed a weighted average of the FA and RD measures on each node of each fiber belonging to the fiber bundle of interest, generating a FA tract profile and a RD tract profile for each subject in the analysis.

To compare the FA and RD tracts profiles between A.D. and controls, we used a modified *t*-test [38]. Specifically, we used the Revised Standardized Difference Test (RSDT) to calculate whether there were differences between A.D.'s and the controls' FA and RD tract profiles at each individual node along the mean core tract and for each fiber bundle of interest. The RSDT takes as input the patient's results, as well as control participants' mean, standard deviation, and the correlation between control participants' scores on the two conditions.

Functional data and processing

To assess whether A.D. had face-selective responses in posterior ventral regions, 23 healthy young adults (mean age = 21.6 years, SD = 3.9 years, range = 18 – 33 years; 16 females, and 7 males) were recruited for an fMRI experiment (see Figure S3). Control participants were part of the student population of the Faculty of Psychology and Educational Sciences of the University of Coimbra, gave written consent to their participation according to established ethical procedures, and received course credit for their participation. The use of healthy young adults as

controls in neuropsychological studies of face perception is relatively common [39], as neural responses to faces are relatively stable across adulthood [40].

In the experiment, we used grayscale photographs of tools, animals, famous faces, and famous places, plus phase-scrambled versions of these stimuli as experimental stimuli [41-44]. Stimuli were presented on a gray background using an Avotec projector with 60 Hz refresh rate. To control stimulus presentation, we used "A Simple Framework" [45] under MATLAB R2014a. Stimuli were back-projected on a screen that A.D. and the control participants viewed with a mirror attached to the head coil. Participants viewed the images passively in a block design. Each run was divided into 6-second miniblocks. In each miniblock, twelve stimuli of the same category were presented for 500 ms without any inter-stimulus interval. Each of these miniblocks was followed by a 6-second fixation block. Eight miniblocks of intact images (two per category), and four miniblocks of the phase-scrambled versions of the images were presented per run. Within each run, miniblocks were pseudo-randomized. A.D. completed 2 runs of this experiment whereas the young controls completed five runs of this experiment. One run lasted 3 minutes and 6 seconds.

We used a T2*-weighted gradient echo echo planar imaging (EPI) sequence (TR = 2000 ms, TE = 30 ms, FoV = 256 × 256, matrix size = 64 × 64, $\alpha = 90°$, BW = 1562 Hz/px). Each image volume consisted of 30 contiguous transverse slices recorded in interleaved slice order oriented parallel to the line connecting the anterior commissure to the posterior commissure covering the whole brain. Before preprocessing, the first two volumes of each run were discarded to allow for T1 saturation effects.

fMRI data were analyzed with the BrainVoyager software package (Version 2.8.2) as well as in-house scripts drawing on the BVQX toolbox written in MATLAB (http://support.brainvoyager.com/available-tools/52-matlab-tools-bvxqtools/232-getting-started.html). Preprocessing of the functional data included, in the following order, slice scan time correction (sinc interpolation), 3D motion correction with respect to the first volume of the first functional run, and linear trend removal in the temporal domain (cutoff: 2 cycles within the run). Functional data were registered (after contrast inversion of the first volume) to high-resolution deskulled anatomy on a participant-by-participant basis in native space. For each participant, echo-planar and anatomical volumes were transformed into Talairach space [46]. All functional data were smoothed at 6mm FWHM (1.5 voxels) and interpolated to 3mm x 3mm voxels. The general linear model was used to fit beta estimates to the experimental events of interest. Experimental events were convolved with a standard 2-gamma hemodynamic response function. The first derivatives of 3D motion correction from each run were added to all models as regressors of no interest to attract variance attributable to head movement.

We localized core face regions for A.D. and for the young controls using the whole-brain contrast of 'Faces > Places'. For A.D., we identified the four core regions (bilateral fusiform face areas and bilateral occipital place areas) individually, whereas for the young controls we used group-level maps from a GLM analysis that treated participants as a random factor. We visually

compared A.D.'s face-selective regions to the controls' face selective regions for size and location.

KEY RESOURCES TABLE

REAGENT or RESOURCE	SOURCE	IDENTIFIER
Deposited Data		
Dataset	This paper	N/A
Face stimuli experiment 1	Michael Tarr	https://wiki.cnbc.cmu.edu/Face_Place
Face stimuli experiment 2	Stirling face database	http://pics.stir.ac.uk/
Software and Algorithms		
R software version 3.6.1	R core team	https://cran.r-project.org/bin/windows/base/old/3.6.1/
MRDIFFUSION Vistasoft package	VISTA Lab	https://github.com/vistalab/vistasoft/
SPM5	Wellcome Centre for Human Neuroimaging	https://www.fil.ion.ucl.ac.uk/spm/software/spm5/
Automatic Fiber Quantification (AFQ)	Yeatman Lab	https://github.com/yeatmanlab/AFQ
A Simple Framework (ASF)	Jens Schwarzbach	https://github.com/jvschw/asf
Matlab R2014	Mathworks	https://www.mathworks.com
BrainVoyager	Brain Innovation	https://www.brainvoyager.com/
BVQX toolbox	Brain Innovation	http://support.brainvoyager.com/available-tools/52-matlab-tools-bvxqtools/232-getting-started.html

References

1. Tadin, D., Lappin, J.S., Blake, R., and Grossman, E.D. (2002). What constitutes an efficient reference frame for vision? Nat Neurosci *5*, 1010-1015.
2. Caramazza, A., and Hillis, A.E. (1990). Levels of representation, co-ordinate frames, and unilateral neglect. Cognitive Neuropsychology *7*, 391-445.
3. Caramazza, A., and Hillis, A.E. (1990). Spatial representation of words in the brain implied by studies of a unilateral neglect patient. Nature *346*, 267-269.
4. Hillis, A.E., and Caramazza, A. (1995). A framework for interpreting distinct patterns of hemispatial neglect. Neurocase *1*, 189-207.
5. Medina, J., Kannan, V., Pawlak, M.A., Kleinman, J.T., Newhart, M., Davis, C., Heidler-Gary, J.E., Herskovits, E.H., and Hillis, A.E. (2009). Neural substrates of visuospatial processing in distinct reference frames: evidence from unilateral spatial neglect. Journal of cognitive neuroscience *21*, 2073-2084.
6. Biederman, I., and Kalocsai, P. (1997). Neurocomputational bases of object and face recognition. Philos Trans R Soc Lond B Biol Sci *352*, 1203-1219.
7. Jiang, F., Blanz, V., and O'Toole, A.J. (2009). Three-dimensional information in face representations revealed by identity aftereffects. Psychological Science *20*, 318-325.
8. Blanz, V., and Vetter, T. (1999). A morphable model for the synthesis of 3D faces. In Proceedings of the 26th annual conference on Computer graphics and interactive techniques. (ACM Press/Addison-Wesley Publishing Co.), pp. 187–194.
9. Taigman, Y., Yang, M., Ranzato, M.A., and Wolf, L. (2014). Web-Scale Training for Face Identification. arXiv.
10. Grüsser, O.-J., and Landis, T. (1991). Visual agnosias and other disturbances of visual perception and cognition, (London: Macmillan).
11. Funatsu, N., Hayakawa, M., Tokuda, N., and Toyoda, K. (2017). Transient Prosopometamorphopsia Restricted to the Left Eye Caused by Ischemia at the Right Splenium of the Corpus Callosum. Intern Med *56*, 2933-2935.
12. Young, A.W., Hellawell, D., and Hay, D.C. (1987). Configurational Information in Face Perception. Perception *16*, 747-759.
13. Moscovitch, M., Winocur, G., and Behrmann, M. (1997). What Is Special about Face Recognition? Nineteen Experiments on a Person with Visual Object Agnosia and Dyslexia but Normal Face Recognition. Journal of Cognitive Neuroscience *9*, 555-604.
14. Rivest, J., Moscovitch, M., and Black, S. (2009). A comparative case study of face recognition: The contribution of configural and part-based recognition systems, and their interaction. Neuropsychologia *47*, 2798-2811.
15. Young, A.W., de Haan, E.H.F., Newcombe, F., and Hay, D.C. (1990). Facial neglect. Neuropsychologia *28*, 391-415.
16. Nagaishi, A., Narita, T., Gondo, Y., Nakane, S., Fukudome, T., and Matsuo, H. (2015). Left-sided metamorphopsia of the face and simple objects caused by an infarction at the right side of the splenium of the corpus callosum. Rinsho Shinkeigaku *55*, 465-471.
17. Hishizawa, M., Tachibana, N., and Hamano, T. (2015). A case of left hemifacial metamorphopsia by a right retrosplenial infarction. Rinsho Shinkeigaku *55*, 87-90.

18. Rangarajan, V., Hermes, D., Foster, B.L., Weiner, K.S., Jacques, C., Grill-Spector, K., and Parvizi, J. (2014). Electrical Stimulation of the Left and Right Human Fusiform Gyrus Causes Different Effects in Conscious Face Perception. The Journal of Neuroscience *34*, 12828.
19. Zhan, J., Ince, R.A.A., van Rijsbergen, N., and Schyns, P.G. Dynamic Construction of Reduced Representations in the Brain for Perceptual Decision Behavior.
20. Freiwald, W.A., and Tsao, D.Y. (2010). Functional compartmentalization and viewpoint generalization within the macaque face-processing system. Science *330*, 845-851.
21. Freiwald, W.A., Tsao, D.Y., and Livingstone, M.S. (2009). A face feature space in the macaque temporal lobe. Nat Neurosci *12*, 1187-1196.
22. Folstein, M.F., Folstein, S.E., and McHugh, P.R. (1975). "Mini-mental state": A practical method for grading the cognitive state of patients for the clinician. Journal of Psychiatric Research *12*, 189-198.
23. Guerreiro, M., Silva, A.P., Botelho, M.A., Leitão, O., Castro-Caldas, A., and Garcia, C. (1994). Adaptação a população portuguesa da tradução do Mini Mental State Examination (MMSE). Revista Portuguesa de Neurologia *1*, 9-10.
24. Freitas, S., Simões, M.R., Alves, L., and Santana, I. (2015). The Relevance of Sociodemographic and Health Variables on MMSE Normative Data. Applied Neuropsychology: Adult *22*, 311-319.
25. Benton, A., De Hamsher, K., Varney, N., and Spreen, O. (1992). Testi di riconoscimentodi volti ignoti, (Firenze: Organizzazioni Speciali).
26. Froming, K., Levy, M., Schaffer, S., and Ekman, P. (2006). The Comprehensive Affect Testing System, (Sharpsburg: Psychology Software Inc.).
27. Righi, G., Peissig, J.J., and Tarr, M.J. (2012). Recognizing disguised faces. Visual Cognition *20*, 143-169.
28. Team, R.C. (2019). R: A Language and Environment for Statistical Computing. (Vienna, Austria: R Foundation for Statistical Computing).
29. Agresti, A. (2002). Categorical Data Analysis. 2nd Edition. (New York: Wiley), pp. 91-101.
30. Yates, F. (1984). Tests of Significance for 2 × 2 Contingency Tables. Journal of the Royal Statistical Society: Series A (General) *147*, 426-449.
31. Rohde, G.K., Barnett, A.S., Basser, P.J., Marenco, S., and Pierpaoli, C. (2004). Comprehensive approach for correction of motion and distortion in diffusion-weighted MRI. Magnetic Resonance in Medicine *51*, 103-114.
32. Friston, K.J., and Ashburner, J. (2004). Generative and recognition models for neuroanatomy. NeuroImage *23*, 21-24.
33. Basser, P.J., and Pierpaoli, C. (2011). Microstructural and physiological features of tissues elucidated by quantitative-diffusion-tensor MRI. Journal of Magnetic Resonance *213*, 560-570.
34. Winklewski, P.J., Sabisz, A., Naumczyk, P., Jodzio, K., Szurowska, E., and Szarmach, A. (2018). Understanding the Physiopathology Behind Axial and Radial Diffusivity Changes—What Do We Know? Frontiers in Neurology *9*.
35. Yeatman, J.D., Dougherty, R.F., Myall, N.J., Wandell, B.A., and Feldman, H.M. (2012). Tract Profiles of White Matter Properties: Automating Fiber-Tract Quantification. PLOS ONE *7*, e49790.

36. Basser, P.J., Pajevic, S., Pierpaoli, C., Duda, J., and Aldroubi, A. (2000). In vivo fiber tractography using DT-MRI data. Magnetic Resonance in Medicine *44*, 625-632.
37. Wakana, S., Caprihan, A., Panzenboeck, M.M., Fallon, J.H., Perry, M., Gollub, R.L., Hua, K., Zhang, J., Jiang, H., Dubey, P., et al. (2007). Reproducibility of quantitative tractography methods applied to cerebral white matter. NeuroImage *36*, 630-644.
38. Crawford, J.R., Garthwaite, P.H., and Porter, S. (2010). Point and interval estimates of effect sizes for the case-controls design in neuropsychology: Rationale, methods, implementations, and proposed reporting standards. Cognitive Neuropsychology *27*, 245-260.
39. Rossion, B., Caldara, R., Seghier, M., Schuller, A.-M., Lazeyras, F., and Mayer, E. (2003). A network of occipito-temporal face-sensitive areas besides the right middle fusiform gyrus is necessary for normal face processing. Brain *126*, 2381-2395.
40. Brodtmann, A., Puce, A., Syngeniotis, A., Darby, D., and Donnan, G. (2003). The functional magnetic resonance imaging hemodynamic response to faces remains stable until the ninth decade. NeuroImage *20*, 520-528.
41. Lee, D., Mahon, B.Z., and Almeida, J. (2019). Action at a distance on object-related ventral temporal representations. Cortex *117*, 157-167.
42. Almeida, J., Martins, A.R., Bergström, F., Amaral, L., Freixo, A., Ganho-Ávila, A., Kristensen, S., Lee, D., Nogueira, J., and Ruttorf, M. (2017). Polarity-specific transcranial direct current stimulation effects on object-selective neural responses in the inferior parietal lobe. Cortex; a journal devoted to the study of the nervous system and behavior *94*, 176-181.
43. Fintzi, A.R., and Mahon, B.Z. (2013). A Bimodal Tuning Curve for Spatial Frequency Across Left and Right Human Orbital Frontal Cortex During Object Recognition. Cerebral Cortex *24*, 1311-1318.
44. Ruttorf, M., Kristensen, S., Schad, L.R., and Almeida, J. (2019). Transcranial Direct Current Stimulation Alters Functional Network Structure in Humans: A Graph Theoretical Analysis. IEEE Trans Med Imaging *38*, 2829-2837.
45. Schwarzbach, J. (2011). A simple framework (ASF) for behavioral and neuroimaging experiments based on the psychophysics toolbox for MATLAB. Behavior Research Methods *43*, 1194-1201.
46. Talairach, J., and Tournoux, P. (1988). Co-planar Stereotaxic Atlas of the Human Brain, (Thieme).

Face-centered representations

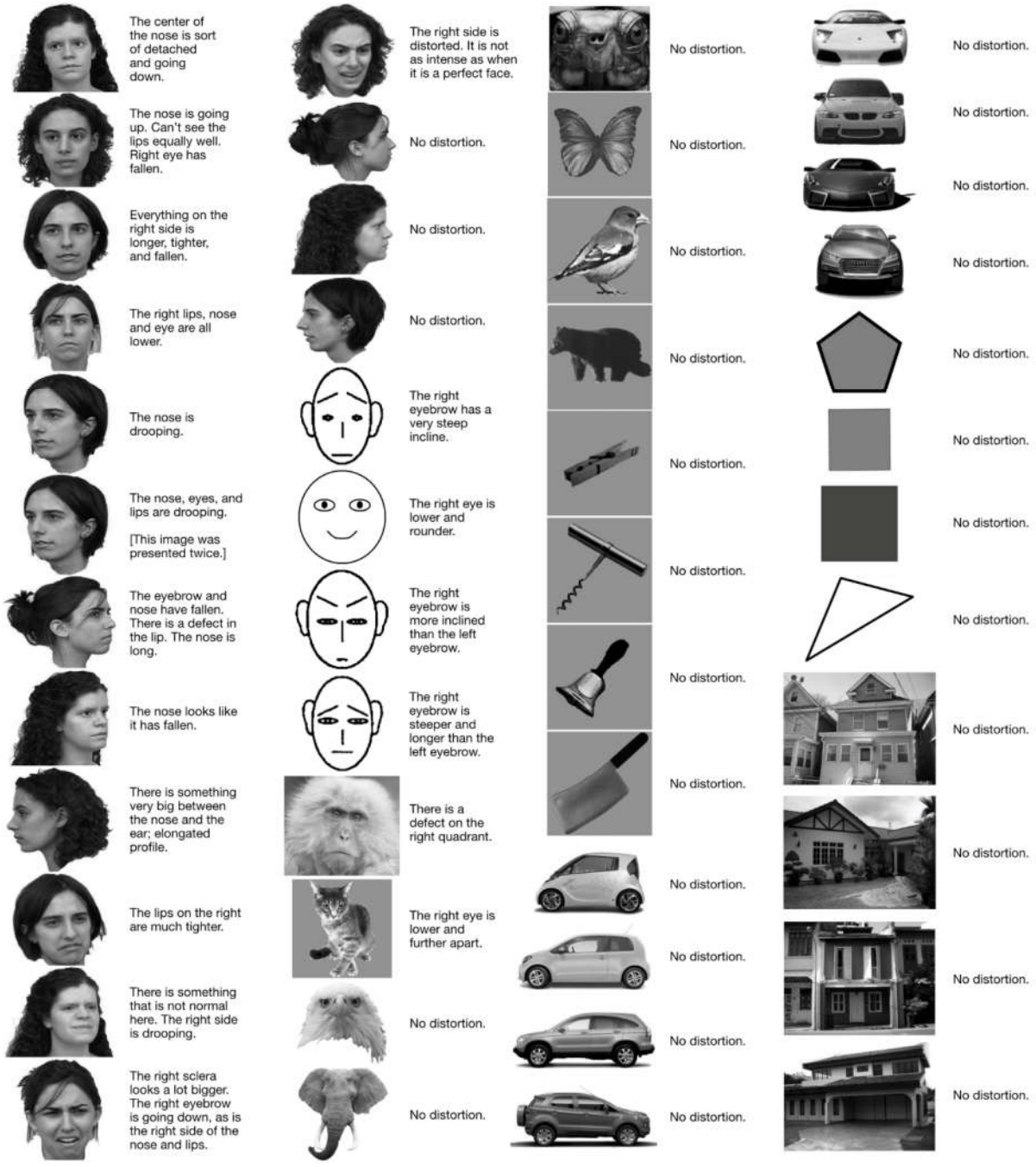

Figure S1. Images presented to A.D. in Experiment 1 along with a description of the distortions that A.D. reported. Related to Figure 3.
The descriptions have been translated from Portuguese to English and paraphrased.

Face-centered representations

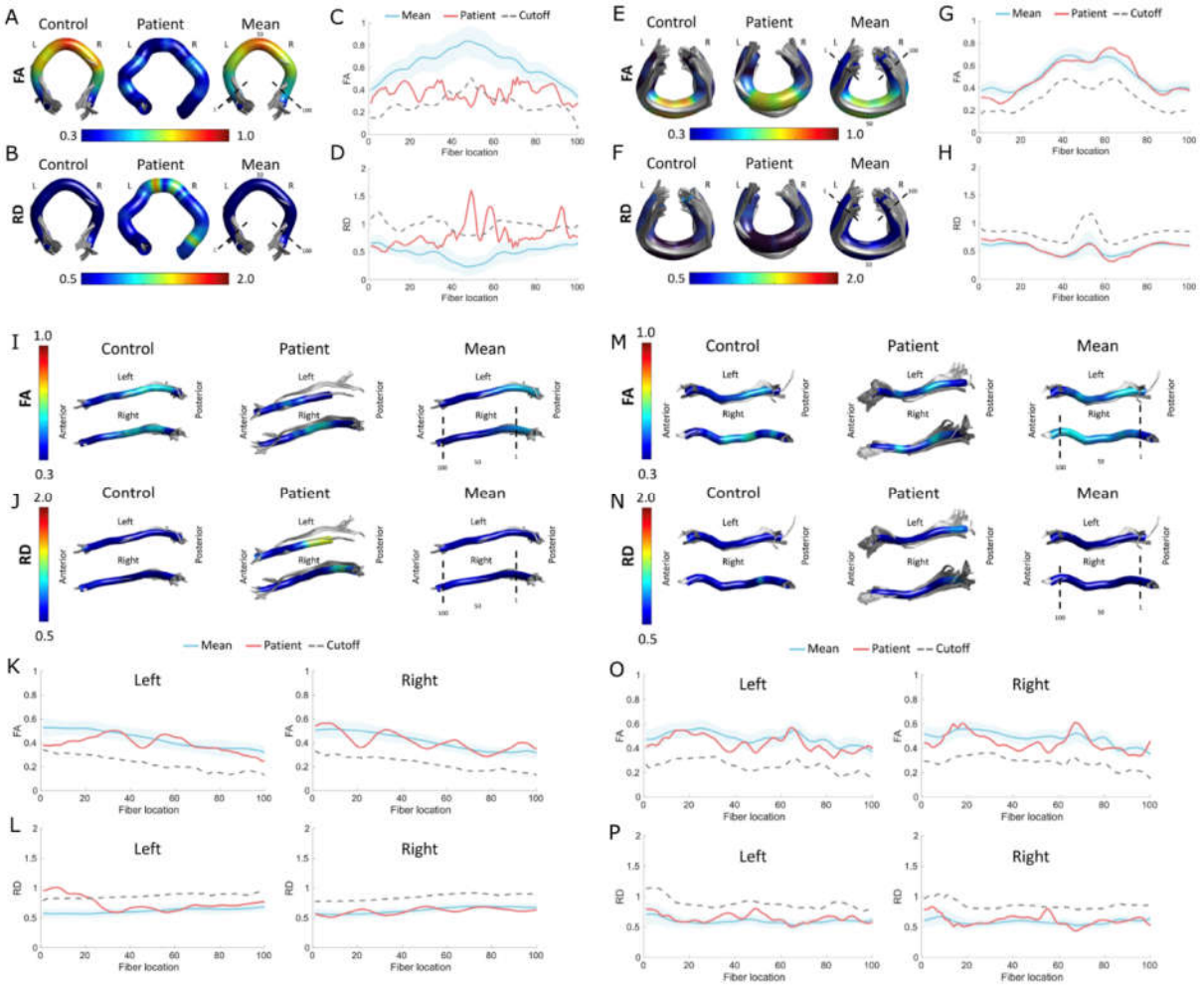

Figure S2. FA and RD tract profiles of A.D. and controls. Related to STAR Methods (DTI Data and processing).

(A) – (D) show data for the forceps major, (E) – (H) show data for the forceps minor, (I) – (L) show data for the left and right inferior longitudinal fasciculi, and (M) – (P) show data for the left and right inferior fronto-occipital fasciculi. (A), (B), (E), (F), (I), (J), (M), and (N) show the three-dimensional rendering of the FA and RD tract profiles for a single representative control, A.D., and the mean tract profile of controls (N = 50). L and R stand for left and right, respectively, and the black dashed lines indicate the equidistant nodes dividing the mean core tract (beginning at node number 1, passing by node number 50 and ending at node number 100). (C), (D), (E), (F), (K), (L), (O), and (P) show FA and RD tract profiles values distribution along the mean core tract at each of the 100 nodes. The red line represents the measured FA and RD for A.D. along the mean core tract; the blue line represents the mean of the measures of all controls, with the shaded blue area indicating one standard deviation apart from the mean. The light gray dashed line represents the minimum FA and the maximum RD values whose *p*-values associated with the RSDT test are less than 0.05 (Bonferroni corrected).

Face-centered representations

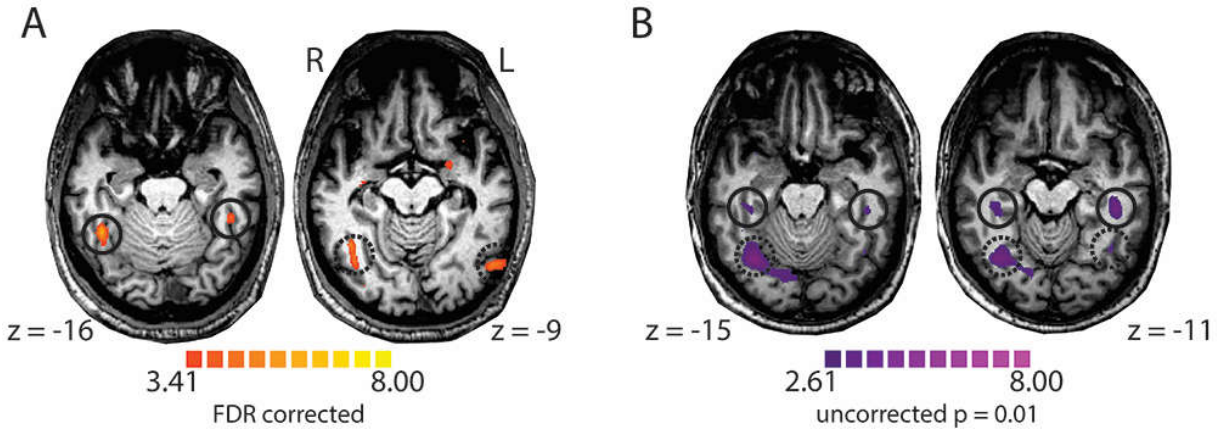

Figure S3. Bilateral fusiform face area and occipital face area in typical face regions for A.D. and young controls. Related to STAR Methods (Functional Data and processing).

t-maps showing the contrast Faces versus Places for (A) A.D. and (B) the young controls in Talairach space. The z coordinate of each axial slice is presented. Solid black circles indicate the fusiform face areas; dashed black circles indicate the occipital face areas.

Face-centered representations

Test	Subpart	Stimulus	# Distorted	# Not Distorted	Comparison	p-value
Experiment 1		Human Faces	17	3	—	—
		Non-Faces	0	20	vs Human Faces	**< 0.000001**
		Animals	2	6	vs Human Faces	**0.004844**
Experiment 2	Visual Field	Left Visual Field	9	0	—	—
		Right Visual Field	6	1	vs Left Visual Field	1
	Face Half	Left Half	1	7	—	—
		Right Half	8	1	vs Left Half	**0.003373**
	Rotation In-plane (Any Distortion)	0 Degrees	15	0	—	—
		90 Degrees	11	4	vs 0 Degrees	0.09962
		180 Degrees	15	0	vs 0 Degrees	1
		270 Degrees	12	3	vs 0 Degrees	0.2241
	Rotation In-plane (Right Side Distortion)	0 Degrees	15	0	—	—
		90 Degrees	11	0	vs 0 Degrees	1
		180 Degrees	15	0	vs 0 Degrees	1
		270 Degrees	10	2	vs 0 Degrees	0.188

Table S1. Behavioral data and statistical comparisons. Related to Figures 3 and 4.
Gray rows indicate the baseline condition, against which the other conditions for a particular test were compared. A two-sided Fisher's exact test was used for all seven comparisons. Bold *p*-values indicate significance at a Bonferroni-corrected alpha value of 0.05 (i.e., 0.05 / 10 = 0.005). The data for the rotation in-plane (right side distortion) subtest is a subset of the rotation in-plane (any distortion) data. For each of the trials where a distortion was reported in the "rotation in-plane (any distortion)" subtest, the "rotation in-plane (right side distortion)" shows whether that distortion was to the right side of the face (i.e. the right was distorted) or the left side of the face (i.e. the right was not distorted).